Investigating the fast response of precipitation intensity to atmospheric heating using a cloud-resolving model

Xin Rong Chua[1], Yi Ming[1,2], Nadir Jeevanjee[3]

[1]Program in Atmospheric and Oceanic Sciences, Princeton University, Princeton, New Jersey, USA
[2]Geophysical Fluid Dynamics Laboratory, Princeton, New Jersey, USA
[3]Department of Geosciences, Princeton University, Princeton, New Jersey, USA

Key Points:

- Atmospheric heating preferentially reduces weak precipitation.
- The intensity of strong precipitation events is maintained by a cancellation between thermodynamic and dynamic effects.
- Free-tropospheric heating warms the boundary layer mainly through reducing rain re-evaporation.

Corresponding author: Xin Rong Chua, `xchua@princeton.edu`

Abstract

Coarse-resolution global climate models cannot explicitly resolve the tropical precipitation intensity distribution, and possible changes caused by forcings. We use a cloud-resolving model to study how imposed atmospheric radiative heating (such as that caused by greenhouse gases or absorbing aerosols) may alter precipitation intensity in a radiative-convective equilibrium setting. It is found that the decrease in total precipitation is realized through reducing weak events (< 400 mm day^{-1}). The intensity of strong precipitation events is maintained by a cancellation between thermodynamic and dynamic effects. A boundary layer energy budget analysis suggests that free-tropospheric heating raises boundary layer temperatures mainly through a reduction in rain re-evaporation. This insight leads to a predictive theory for the surface sensible and latent flux changes. The results imply that cloud process play a key role in shaping the temperature and precipitation responses to atmospheric heating.

Plain language summary: The effect of atmospheric heating on precipitation intensity is investigated using a model that can resolve moist convection. It is found that heating the entire atmosphere reduces mean precipitation and elevates water vapor concentration near the surface. The latter increases the fraction of intense rainfall. Decreased mean precipitation also weakens the re-evaporative cooling from falling rain, allowing the heating in the interior of the atmosphere to warm up near-surface air. The results show how important cloud processes are for understanding the temperature and precipitation responses to atmospheric heating.

1 Introduction

Greenhouse gases and absorbing aerosols warm climate by absorbing longwave and shortwave radiation, respectively. Greenhouse gases represent the strongest anthropogenic climate forcing, with top-of-the-atmosphere (TOA) values of 2.54-3.12 W m^{-2} [*Myhre et al.*, 2013]. Unlike well-mixed greenhouse gases, unevenly distributed absorbing aerosols can lead to local TOA forcing exceeding 20 W m^{-2} [e.g. *Strong et al.*, 2015]. The radiative heating gives rise to a fast (days to months) atmosphere-land response and a slow (years or longer) response that involves the ocean [e.g. *Andrews and Forster*, 2010]. Given the different time scales, the two responses can be treated as distinct. In fact, global climate model (GCM) simulations indicate that the fast response to atmospheric absorption acts to reduce global-mean precipitation, while the slow response has the opposite effect [*Andrews et al.*, 2010; *Ming et al.*, 2010; *Fläschner et al.*, 2016]. For this reason, one can study the fast response in isolation from the slow response.

On fast time scales, an increase in atmospheric radiative heating must be balanced partially by a reduction in surface latent heat flux (and mean precipitation) [*Andrews et al.*, 2010; *Bala et al.*, 2010; *Dinh and Fueglistaler*, 2017; *Richardson et al.*, 2015]. This change in mean precipitation need not scale with, or even agree in sign, with those of precipitation extremes. For example, a study of the fast response to doubling CO_2 reported a percentage decrease in tropical cyclone frequency (-10%) that more than doubles that in mean precipitation (-2.3%) over the TC genesis regions [*Held and Zhao*, 2011].

The fast response of precipitation intensity to atmospheric heating has been studied with GCMs. *Sillmann et al.* [2017] found that GCMs do not even agree on the sign of the annual maximum daily precipitation change caused by a quadrupling of CO_2. Besides the lack of consensus among models, there are many well-known reasons to doubt the capability of GCMs in simulating extreme precipitation with parameterized moist convection, especially in the tropics [*O'Gorman*, 2015]. GCMs typically underestimate intense precipitation when compared with observations, with the biases being more severe for low-resolution GCMs (1° or coarser) [*Stephens et al.*, 2010; *Kopparla et al.*, 2013; *Sillmann et al.*, 2013; *O'Brien et al.*, 2016]. While the convective parameterization of a GCM can be altered to better match observations, a troubling sign is that such a modification can lead to larger changes in the frequency of heavy rain than a 2-K increase in sea surface temperatures (SSTs) [*Wilcox and Donner*, 2007], casting in doubt the models' utility in studying extreme precipitation changes.

In light of GCMs' limitations, we turn to cloud-resolving models (CRMs) on a limited-area domain, which have been shown to produce realistic simulations of heavy rain events when forced with proper boundary conditions [*Fan et al.*, 2015; *Lee et al.*, 2016; *Hodzic and Duvel*, 2018]. Since what is at issue here is the general characteristics of the fast response to atmospheric heating, we intentionally move away from detailed simulation of a particular region or event in favor of a setting that is more representative of the climate system, namely radiative-convective equilibrium (RCE). One advantage of RCE is that both energy and moisture are conserved within the atmosphere, which need not be the case for individual events. One can think of RCE as an approximation of the tropical climate without large-scale mean circulation.

The troposphere consists of the free troposphere and boundary layer. In this paper, we analyze their energy balances separately to better identify the physical mechanisms through which elevated heating affects boundary layer properties (such as temperature and humidity). A specific issue to be addressed is the boundary layer energetics. Existing works have focused on the balance among sensible heating, radiative cooling and entrainment of free-tropospheric air into the boundary layer [*Ball*, 1960; *Lilly*, 1968]. The entrainment term is often parameterized as a fixed fraction of the surface sensible heat flux [0.2 or 0.25 in *Betts*, 1973; *Tennekes*, 1973; *Betts and Ridgway*, 1989; *Betts*, 2000; *Cronin*, 2013], implying that the sensible heat flux is tightly coupled to the boundary layer radiative cooling. While *Betts* [2000] later recognized that precipitation re-evaporative cooling might contribute to the boundary layer energy balance, possible change in re-evaporation under warming is not taken into account explicitly in the analytical models of climate sensitivity [*Takahashi*, 2009; *Cronin*, 2013]. This means that the boundary layer energy balance, and for that reason boundary layer temperature are, to first order, independent of free-tropospheric heating. This paper will test the validity of this assumption.

2 Methods

We use the Advanced Research Weather Research and Forecasting (WRF) model configured to run in RCE [*Wang and Sobel*, 2011]. Radiative transfer is reduced to a prescribed cooling rate in the troposphere ($T > 207.5K$), and Newtonian relaxation in the stratosphere to 200K on a time scale of 5 days [*Pauluis and Garner*, 2006]. This highly idealized radiation scheme allows us to focus on the effects of imposed atmospheric heating without complicating factors such as water vapor feedback and cloud radiative effect. Sub-grid diffusion is parameterized following the YSU boundary layer scheme [*Hong et al.*, 2006] in the vertical direction, and the Smagorinsky two-dimensional scheme in the horizontal. The single-moment Purdue-Lin microphysics scheme [*Lin et al.*, 1983; *Rutledge and Hobbs*, 1984; *Chen and Sun*, 2002] contains six species: water vapor, cloud water, cloud ice, rain, snow and graupel. Surface sensible and latent heat fluxes (SH and LH, respectively; both in W m^{-2}) are calculated using the bulk aerodynamic formula with a drag coefficient of 0.001 and a constant near-surface wind speed of 5 m s^{-1}:

$$SH = 0.005c_p(T_s - T_a) \tag{1}$$

$$LH = 0.005L(q_{sat} - q_a), \tag{2}$$

where c_p is the specific heat capacity of air (1004.5 J kg^{-1} K^{-1}), L the latent heat of vaporization (2.5×10^6 J kg^{-1}), T_s surface temperature, T_a the lowest model level (or near-surface) temperature, q_{sat} the saturated water vapor mixing ratio at T_s, and q_a the lowest model level water vapor mixing ratio. Note that the density of air in the boundary layer is set at 1 kg m^{-3} for the purpose of calculating surface fluxes. As T_s and q_{sat} are fixed, it is clear from Eqs. 1 and 2 that the only way to alter SH and LH is by adjusting near-surface boundary layer temperature and humidity (T_a and q_a).

All simulations are performed on a doubly-periodic domain of 96$\times$ 96 gridpoints with a horizontal spacing of 2 km. There are fifty vertical levels, nine of which are in the lowest 1 km. Domain-average winds are relaxed to zero on a time scale of 2 hours to prevent wind shear from developing, similar to *Tompkins and Semie* [2017]. The surface temperature is set at 301.15 K, making the lower boundary conditions horizontally homogenous. The two control simulations wth different microphysical assumptions (to be discussed) are initialized with a warm bubble and are performed for 240 model days; the perturbation simulations are branched off day 180 of their respective controls and last 60 model days. The last 20 days of hourly-mean outputs from each simulation are analyzed. We use five consecutive, non-overlapping 20-day periods (days 220-320) for assessing the noise level of any given variable. The difference between a control and a perturbation is considered significant if it rises above the noise level.

The prescribed radiative cooling rate is at the default value (-1.5 K day^{-1}) in the first base case (BASE). It is reduced by half to -0.75 K day^{-1} throughout the troposphere in HEAT. To isolate the boundary layer response to free-tropospheric heating, we separate the uniform radiative heating into two complementary cases: halving the cooling only above 850 hPa (A850) and below (B850). To assess the importance of rain re-evaporation in communicating free-tropospheric heating to the boundary layer, we repeat all the simulations with a model configuration in which the rate of rain re-evaporation in the cloud microphysics module is arbitrarily suppressed by a factor of 10. The four additional cases are denoted by adding an asterisk to the original case names. We will refer to the two groups of experiments as full and partial re-evaporation, respectively. Throughout this paper, a response to heating is denoted with a δ.

3 Results

3.1 Domain-average responses

Table 1. Domain-average tropospheric radiative cooling (RA, W m^{-2}), surface sensible heat flux (SH, W m^{-2}), surface latent heat flux (LH, W m^{-2}), near-surface temperature (T_a, K) and water vapor mixing ratio (q_a, 10^{-3} kg kg^{-1}), precipitation (P, mm day^{-1}), and changes in the perturbation cases. All changes are significant.

	RA	SH	LH	T_a	q_a	P
BASE	-145	19.5	127	297.3	14.4	4.4
δHEAT	72	-14.7	-55.1	2.9	4.3	-1.9
δA850	59	-11.1	-46	2.2	3.6	-1.6
δB850	13	-4.2	-7.8	0.84	0.61	-0.27
BASE*	-145	9.4	137	299.3	13.6	4.7
δHEAT*	72	-9.3	-61.2	1.8	4.8	-2.1
δA850*	59	-4.7	-53.2	0.95	4.2	-1.8
δB850*	13	-6.3	-5.7	1.3	0.45	-0.2

We begin by examining a set of key domain-average quantities and their changes resulting from forced heating (Table 1). Relative to BASE, the tropospheric radiative cooling (from the surface to 200 hPa) is cut by half in HEAT. The resulting net heating is balanced by reducing both surface sensible and latent heat fluxes with a ratio of δSH to δLH at 0.27, which differs significantly from the Bowen ratio in BASE (0.15), suggesting that radiative cooling plays a role in determining the Bowen ratio. Consistent with Eqs. 1 and 2, the near-surface temperature (T_a) increases by 2.9 K, while the near-surface water vapor mixing ratio (q_a) increases by 30%. [The latter is greater than what one would expect from the Clausius-Clapeyron relation and assuming constant relative humidity (RH) (20%). Indeed, the near-surface RH increases by about 10% (relative change) to make up the difference.] More quantitatively, according to Eqs. 1 and 2, the changes in SH (δSH) and LH (δLH) can be written as $-0.005c_p\delta T_a$ and $-0.005L\delta q_a$, respectively, meaning that one can tie the near-surface temperature and humidity changes directly to imposed heating. It is, nonetheless, unclear what determines the relative contributions of sensible and latent heating, a point to which we will return in Section 3.3. The domain-average precipitation (equivalent to latent heat flux) reduces by 43%, which is less than the relative decrease in radiative cooling.

For the two differential heating cases, the column-integrated change in radiative cooling in A850 is about 4.5 times of that in B850. This is understandable as it is approximately proportional to the pressure depth to which the perturbations are applied [i.e. (850-200)/(1000-850)]. The ratio is 2.6 for δT_a, and 5.9 for δq_a and δP, suggesting that elevated heating is less effective at modifying surface sensible flux (near-surface temperature), but more so at altering surface latent heat flux (near-surface moisture and precipitation). It is still somewhat surprising to see that the free-tropospheric heating has a substantial warming effect on the near surface, especially given that most of the sensible heating from the YSU scheme is placed in the boundary layer. This suggests that when conjecturing a quantitative theory for the partitioning of surface sensible and latent heating, one has to take into account the vertical distribution of atmospheric radiative heating and the coupling between the free troposphere and boundary layer.

Relative to BASE, the decreased microphysical cooling in BASE* warms the boundary layer by 2 K, reducing the surface sensible heat. The tropospheric energy balance is restored by increasing the surface latent heat flux, which is consistent with lower boundary layer humidity. The response of sensible heat to the heating in HEAT* is much smaller (-9.3 W m^{-2}) than that of HEAT (-14.7 W m^{-2}). Note that the surface sensible heat flux is close to zero in HEAT*. As compared to the full re-evaporation counterparts, elevated heating becomes less effective in inducing boundary layer warming (1.8 K in HEAT* versus 2.9 K in HEAT, and 0.95 in A850* versus 2.2 K in A850). Consequently, the reduction in latent heat (precipitation) is more pronounced in the partial re-evaporation cases with free-tropospheric heating.

Figure 1 shows the vertical profiles of temperature (T), water vapor mixing ratio (q), equivalent potential temperature (θ_e) and cloud fraction in BASE (top row) and their changes in the perturbation cases (bottom row). The temperature structure in RCE follows that of a moist adiabat (Figure 1a), and to first order sets the vertical structure of water vapor (Figure 1b) in the free troposphere. θ_e shows a first baroclinic structure,

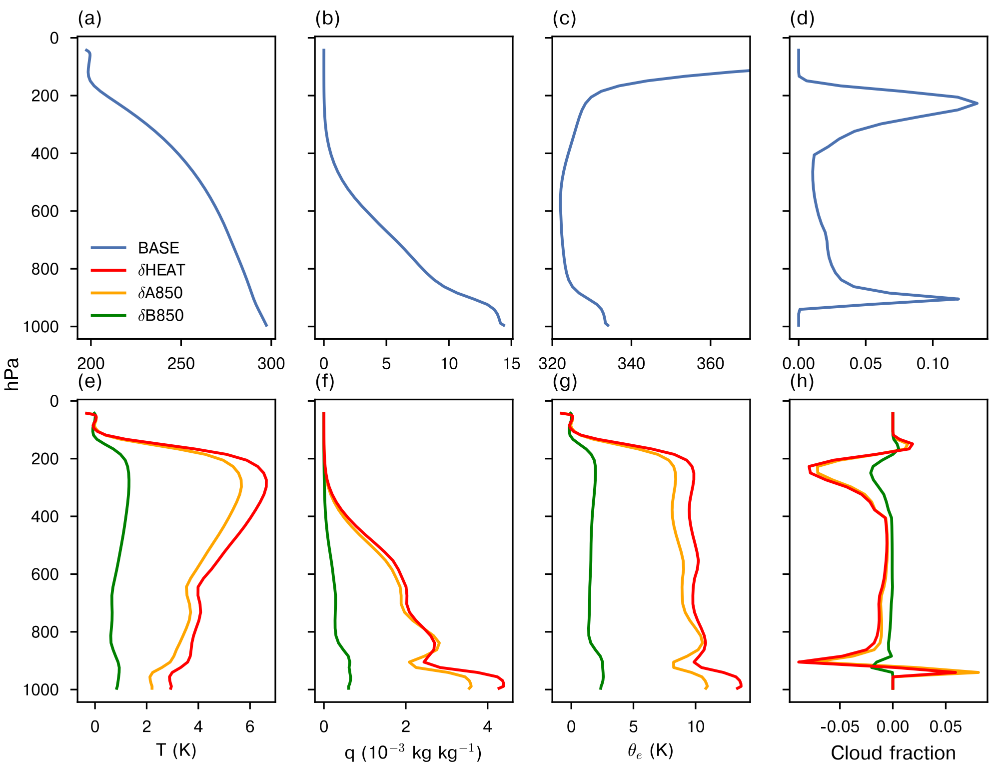

Figure 1. Vertical profiles of (a) temperature (T, K), (b) water vapor mixing ratio (q, 10^{-3} kg kg^{-1}), (c) equivalent potential temperature (θ_e, K), (d) cloud fraction in BASE. (e-h) Changes in (a-d) due to heating (prefixed by δ) in HEAT, A850, and B850. All changes rise significantly above the noise level.

with a minimum at around 500 hPa. Under heating, the near-surface warming extends throughout the troposphere, with appreciable amplification in the middle and upper troposphere, as a consequence of moist adiabatic control (Figure 1e). In contrast, the accompanying increase in q is bottom-heavy, as in the control (Figure 1f). θ_e increases rather uniformly throughout the troposphere (Figure 1g). As in *Wang and Sobel* [2011], a grid is defined as cloudy if the total cloud condensate (water and ice) exceeds 0.005 g kg^{-1}. Cloud fraction has two maxima in the vertical direction (Figure 1d). One can regard the lower one approximately as the lifting condensation level (LCL). It becomes lower in HEAT as the near-surface RH increases [*Romps*, 2017]. Note that the LCL remains above 950 hPa (the boundary layer top used in this paper) in all experiments. The cloud fraction in HEAT is approximately half of that in BASE (Figures 1d,h).

3.2 Precipitation intensity

The domain-average precipitation of the events at gridpoints where the hourly precipitation rate r exceeds a threshold value r_t (in mm day^{-1}), is denoted as $p(r > r_t)$ and shown in Figure 2a. By definition, $p(r > 0)$ is the domain-average precipitation of all events (P), which was discussed in the previous section. In BASE, $p(r > 400)$ is about 0.8 mm day^{-1} (referred to as strong events in this work), while the rest (3.5 mm day^{-1}) is accounted for by weak events (r less than 400 mm day^{-1}). Despite the substantial (43%) reduction in P in HEAT, there is almost no change (+0.1 mm day^{-1}) in the precipitation generated by strong events. Thus, the reduction is realized exclusively by lowering the precipitation from weak events from 3.4 mm day^{-1} in BASE to 1.6 mm day^{-1} in HEAT. This amounts to a 53% decrease.

Figure 2b plots the hourly precipitation rate against 500-hPa vertical velocity (w) for all gridpoints in BASE and HEAT. Both quantities are strongly correlated, especially for the events with appreciable positive (upward) w (greater than ~ 0.1 m s^{-1}); a linear regression through the origin yields $R = 0.67$ for BASE and HEAT. Yet, the slope (k) for HEAT is 34% larger than for HEAT, meaning that the same updraft generates considerably more precipitation in the former. This is consistent with the 30% increase in the average near-surface water vapor mixing ratio (q_a) as discussed above. As such, the strong events in BASE can be thought of approximately as being generated by vertical motions exceeding 2.2 m s^{-1}. In comparison, the threshold stands at 1.7 m s^{-1} in

HEAT. One may also gather that vertical velocity is generally weaker in HEAT than in BASE.

Figure 2c shows the probability of w exceeding a threshold w_t for $w_t > 0.1$ m s^{-1}, or $\int_{w_t}^{\infty} \mathcal{P}(w)dw$, where $\mathcal{P}(w)$ is the probability density function of w. Ascents are relatively rare; on average only 1.0% of the grids have w larger than 0.1 m s^{-1}. The probability decreases by three orders of magnitude as w_t increases to 5 m s^{-1}. In HEAT, ascending motions become even less likely across the entire range of w_t, affirming the impression of weaker ascents from Figure 2b.

To better understand the different responses of strong versus weak events, we write the domain-average precipitation of the events with w greater than a certain positive value w_t [$p(w > w_t)$, w_t in m s^{-1}] approximately as:

$$p(w > w_t) = k \int_{w_t}^{\infty} w\mathcal{P}(w)dw. \tag{3}$$

$p(w > 0.1)$ is 2.3 mm day^{-1} in BASE, which accounts for slightly more than half of the total precipitation (Figure 2d). [The remaining is associated with very weak ascents (less than 0.1 m s^{-1}) and descents.] $p(w > w_t)$ is consistently smaller in HEAT for w_t greater than 0.05 m s^{-1}, making it easier to interpret the difference between the two cases than in terms of $p(r)$ (Figure 2a). To that end, one can linearly decompose the difference [$\delta p(w > w_t)$] into the thermodynamic (δk) and dynamic ($\delta\mathcal{P}$) terms:

$$\delta p(w > w_t) \approx \delta k \int_{w_t}^{\infty} w\mathcal{P}(w)dw + k \int_{w_t}^{\infty} w\delta\mathcal{P}(w)dw. \tag{4}$$

Figure 2e indicates that although this decomposition underestimates the difference between BASE and HEAT, it does capture some important characteristics of the simulations (e.g. $\delta p(w > w_t)$ generally decreases as w_t increases). While the thermodynamic effect owing to higher near-surface water vapor mixing ratio acts to enhance precipitation, the dynamic effect in the form of weaker ascents tends to lower precipitation. As the dynamic effect outweighs the thermodynamic effect, the net result is a reduction of precipitation at a given w_t. To address the question why the precipitation from strong events [$p(r > 400)$] is similar between BASE and HEAT, one also needs to consider that it requires less vigorous ascents to produce these events (defined in terms of r) in HEAT than in BASE. As noted before, the threshold w_t is 1.7 m s^{-1} in HEAT, as opposed to 2.2 m s^{-1} in HEAT. This factor makes up the net reduction of precipitation after the cancellation of the thermodynamic and dynamic effects, resulting in little change in terms of $p(r > 400)$.

3.3 Boundary layer energy balance

Surface sensible heat (SH) is the main energy source for the boundary layer in BASE (Figure 3a). Additional heating is realized through the exchange of sensible heat with the free troposphere, either explicitly resolved or parameterized at the sub-grid scale (EX). The sink terms are radiative cooling (RA_b) and re-evaporative cooling (RE) in the boundary layer. The latter takes place as rain falls through the unsaturated boundary layer and is thus microphysical in nature. Somewhat surprisingly, the magnitude of re-evaporative cooling is larger than that of radiative cooling, which is often presumed to be the dominant sink term.

Figure 3b summarizes how the individual terms vary in the perturbation cases. Although imposed radiative heating is clearly present in HEAT, the main balance is between SH and RE, both of which decrease substantially in magnitude. As A850 and B850 add up roughly to HEAT, one can see that the boundary layer radiative heating is balanced almost entirely by lowering SH, as is the case in B850. The large reduction in RE seen in HEAT can be attributed to the radiative heating above 850 hPa, and amounts to a warming effect on the boundary layer. This is consistent with lower SH and higher near-surface temperature (Table 1). The changes in EX are much smaller than than those in SH in all cases.

One can define precipitation efficiency (ϵ) as the ratio of precipitation (P) over column-integrated condensation (C) [*Zhao*, 2014], with a value of 0.33 in BASE. Re-evaporation, which is equal to the difference between C and P (i.e. $C-P$), can be written as $P(1-\epsilon)/\epsilon$. As ϵ is little changed across the cases (within 0.01), the fractional changes in column-integrated re-evaporation and precipitation should be similar to each other. This relation also holds approximately for boundary layer re-evaporation (i.e. $\delta RE/RE = \delta P/P$), which decreases by 64% in BASE in comparison with a 43% reduction of precipitation.

The partial re-evaporation simulations allow us to further assess the importance of re-evaporation. Despite having the same boundary layer radiative cooling as BASE,

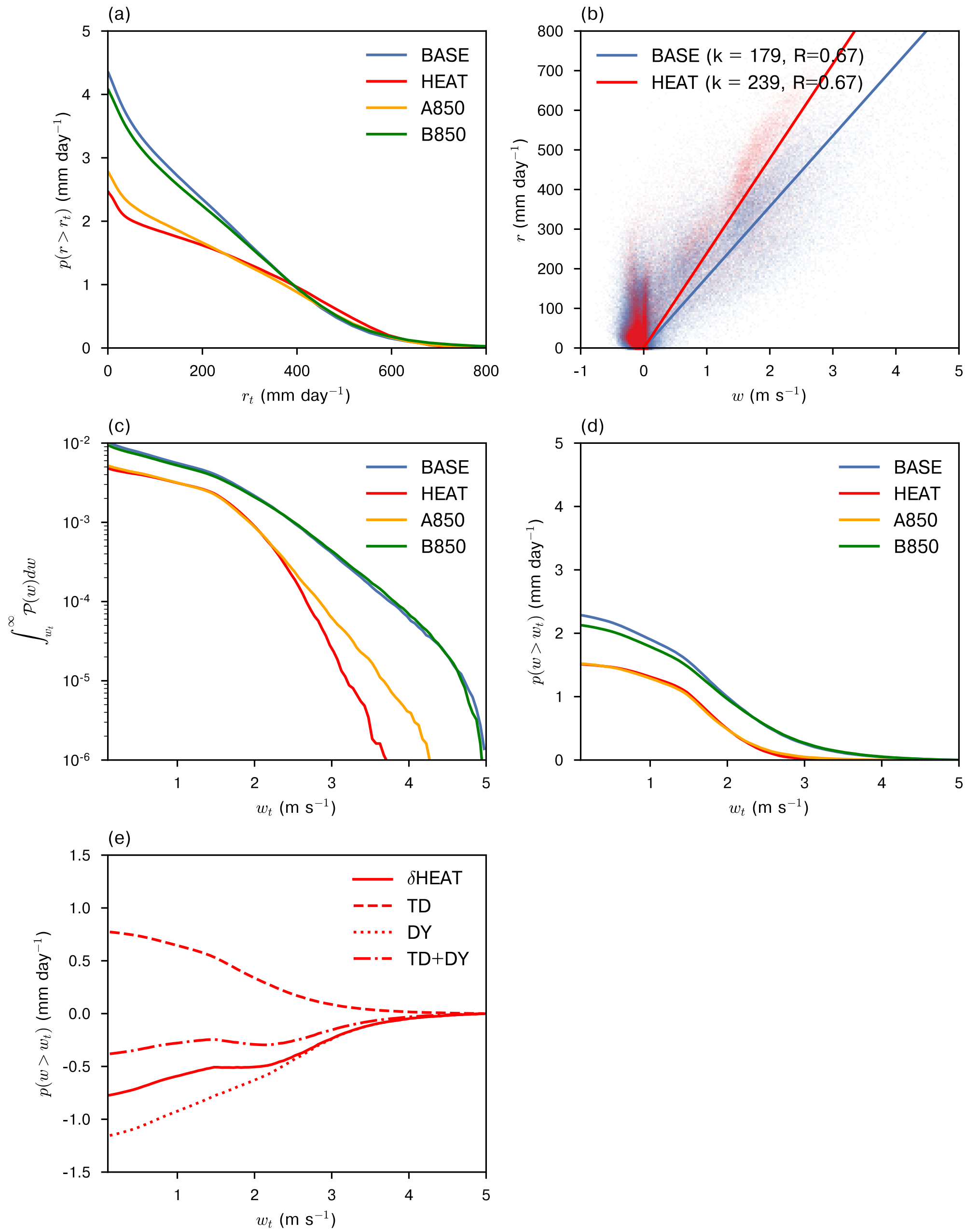

Figure 2. (a) The domain-average precipitation ($p(r>r_t)$, mm day^{-1}) of the events whose hourly precipitation rates exceed r_t (mm day^{-1}) in the full re-evaporation experiments. (b) The scatter plot of r (mm day^{-1}) against 500-hPa vertical velocity (w, m s^{-1}) for BASE and HEAT. The solid lines are the best-fit lines with zero-intercept for $w > 0.1$ m s^{-1}. (c) The probability of w exceeding a threshold w_t (m s^{-1}), or $\int_{w_t}^{\infty} \mathcal{P}(w)dw$, for $w_t > 0.1$. (d) The domain-average precipitation ($p(w>w_t)$, mm day^{-1}) of the events where w exceeds w_t, estimated with Equation 3. (e) The difference in $p(w>w_t)$ between BASE and HEAT, and its thermodynamic and dynamic components and their sum, estimated with Equation 4.

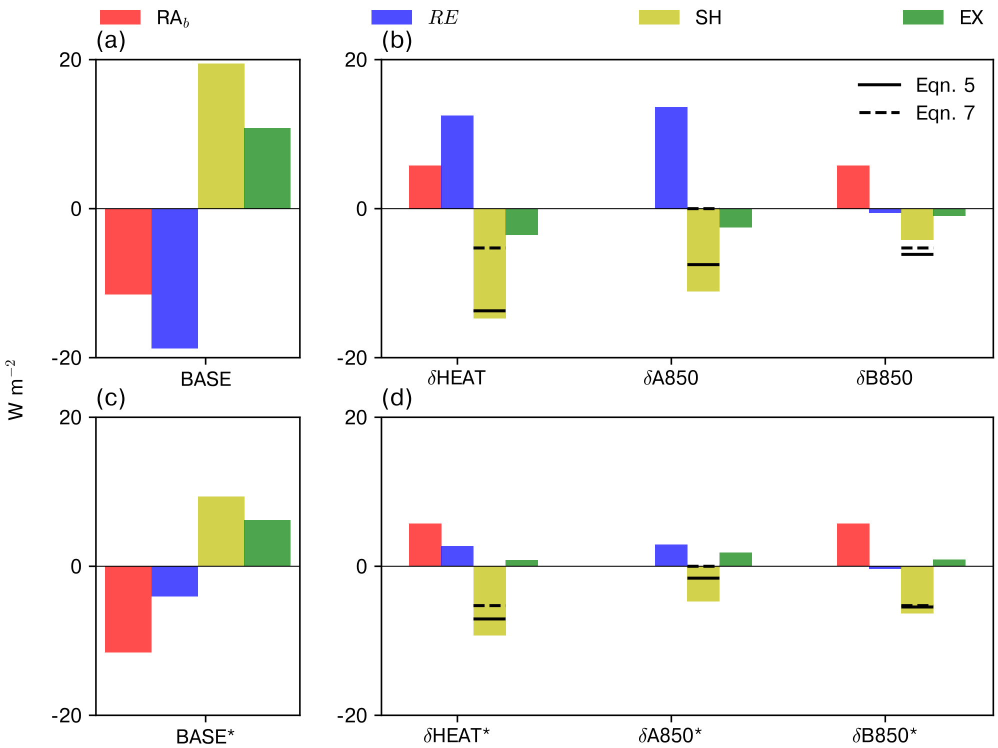

Figure 3. (a) The individual terms in the boundary layer energy balance (W m^{-2}) in BASE: surface sensible heating (SH), radiative cooling (RA_b), re-evaporative cooling (RE) and the exchange of sensible heat with the free troposphere (EX). (b) Changes in HEAT, A850 and B850. (c,d) Same as (a,b), but for the partial re-evaporation cases. The solid and dashed lines denote the change in SH calculated from Equations 5 and 7, respectively.

the magnitudes of the surface sensible heating and the exchange term are much reduced in BASE*, presumably due to the suppressed re-evaporative cooling (Figure 3c). The response to free-tropospheric heating is also muted considerably in A850*; the resulting reduction in SH is less than half of that in A850. The same is true for near-surface temperature (Table 1). This reaffirms the importance of re-evaporative cooling in communicating the effect of free-tropospheric heating to the boundary layer and surface.

4 Discussion and summary

It is clear from the above results that the vertical distribution of radiative heating is key to determining the relative roles of surface sensible and latent heat adjustments in re-establishing the tropospheric energy balance. In particular, re-evaporative cooling is the main process through which the effect of free-tropospheric heating can be felt by the boundary layer and surface. Thus, re-evaporation has to be considered explicitly in any attempt to develop a quantitative theory of the surface turbulent flux response to atmospheric heating.

If one assumes that the free-tropospheric energy balance can be approximated as radiative cooling balancing out latent heating, it follows that the fractional change of precipitation is equal to that of the free-tropospheric radiative cooling ($\delta P/P = \delta RA_f/RA_f$). As discussed before, the fractional change of the boundary layer re-evaporative cooling is approximately equal to that of precipitation. Thus, δRE can be written as $\alpha\delta RA_f$, where α is the ratio of RE to RA_f in the base case. If the exchange term does not vary appreciably with imposed heating, the boundary layer energy balance leads to the following expression of the surface sensible heat flux change:

$$\delta SH = -\delta RA_b - \alpha\delta RA_f. \tag{5}$$

Furthermore, its latent heat counterpart can be derived from the tropospheric energy balance:

$$\delta LH = (\alpha - 1)\delta RA_f. \tag{6}$$

This constitutes a predictive theory of δSH and δLH in response to δRA_b and δRA_f as α (0.13 in BASE) depends only on values in BASE. The predicted δSH is in good agreement with the simulations (Figure 3). According to this theory, free-tropospheric heating reduces latent heating more than sensible heating as long as α is smaller than 0.5. Also, boundary layer heating decreases sensible heating only.

The approximation used in *Takahashi* [2009] and *Cronin* [2013] can be viewed as a special case of Equation 5 with $\alpha = 0$:

$$\delta SH = -\delta RA_b. \tag{7}$$

The partial re-evaporation experiments allow us to test the theory for a small value of α (0.02 in BASE*) that approaches this special case. Indeed, the predictions from Equations 5 and Equation 7 are much closer than for the full experiments. In other words, the $\alpha\delta RA_f$ term in Equation 5 greatly improves the accuracy of the predicted δSH by incorporating the effect of re-evaporation in coupling the boundary layer and the free-troposphere.

In summary, imposed radiative warming reduces domain-average precipitation (evaporation) by increasing boundary layer water vapor, a thermodynamic effect that tends to enhance precipitation rate at a given vertical velocity. This effect opposes the weakening of ascents (a dynamic effect), resulting in no significant change in the precipitation from strong events. The decrease in domain-average precipitation is realized entirely through weak events. A key finding is that free-tropospheric radiative heating affects the boundary layer and surface properties primarily by weakening the re-evaporative cooling. This insight leads to a predictive theory of the surface latent and sensible heat flux changes caused by radiative heating.

Acknowledgments

The source code for the WRF model was provided by Shuguang Wang, who also offered valuable advice on its use. The simulations were performed and archived on NOAA's High Performance Computing System, and are available upon request. The analysis was aided by the “aospy” climate model analysis package developed by Spencer Hill and Spencer Clark. XRC is supported by the Singapore National Research Foundation Environmental and Water Technologies Ph.D. Scholarship and the Cooperative Institute for Modeling the Earth System, and wishes to thank Hailey Shin, Usama Anber, Spencer Clark, Leo Donner and Lucas Harris for helpful discussion. We thank Leo Donner and Levi Silvers for constructive reviews that improved the clarity of the paper.

References

Abbot, D. S. (2014), Resolved snowball Earth clouds, *Journal of Climate*, *27*(12), 4391–4402.

Andrews, T., and P. M. Forster (2010), The transient response of global-mean precipitation to increasing carbon dioxide levels, *Environmental Research Letters*, *5*(2), 025,212.

Andrews, T., P. M. Forster, O. Boucher, N. Bellouin, and A. Jones (2010), Precipitation, radiative forcing and global temperature change, *Geophysical Research Letters*, *37*(14).

Bala, G., K. Caldeira, and R. Nemani (2010), Fast versus slow response in climate change: implications for the global hydrological cycle, *Climate Dynamics*, *35*(2-3), 423–434.

Ball, F. (1960), Control of inversion height by surface heating, *Quarterly Journal of the Royal Meteorological Society*, *86*(370), 483–494.

Betts, A. (1973), Non-precipitating cumulus convection and its parameterization, *Quarterly Journal of the Royal Meteorological Society*, *99*(419), 178–196.

Betts, A. K. (2000), Idealized model for equilibrium boundary layer over land, *Journal of Hydrometeorology*, *1*(6), 507–523.

Betts, A. K., and W. Ridgway (1989), Climatic equilibrium of the atmospheric convective boundary layer over a tropical ocean, *Journal of the Atmospheric Sciences*, *46*(17), 2621–2641.

Bretherton, C. S., P. N. Blossey, and M. Khairoutdinov (2005), An energy-balance analysis of deep convective self-aggregation above uniform SST, *Journal of the Atmospheric Sciences*, *62*(12), 4273–4292.

Chen, S.-H., and W.-Y. Sun (2002), A one-dimensional time dependent cloud model, *Journal of the Meteorological Society of Japan*, *80*(1), 99–118.

Cronin, T. W. (2013), A sensitivity theory for the equilibrium boundary layer over land, *Journal of Advances in Modeling Earth Systems*, *5*(4), 764–784.

Dinh, T., and S. Fueglistaler (2017), Mechanism of fast atmospheric energetic equilibration following radiative forcing by CO_2, *Journal of Advances in Modeling Earth*

Systems, *9*(7), 2468–2482.

Emanuel, K., A. A. Wing, and E. M. Vincent (2014), Radiative-convective instability, *Journal of Advances in Modeling Earth Systems*, *6*(1), 75–90.

Fan, J., D. Rosenfeld, Y. Yang, C. Zhao, L. R. Leung, and Z. Li (2015), Substantial contribution of anthropogenic air pollution to catastrophic floods in Southwest China, *Geophysical Research Letters*, *42*(14), 6066–6075.

Fläschner, D., T. Mauritsen, and B. Stevens (2016), Understanding the intermodel spread in global-mean hydrological sensitivity, *Journal of Climate*, *29*(2), 801–817.

Held, I. M., and M. Zhao (2011), The response of tropical cyclone statistics to an increase in CO_2 with fixed sea surface temperatures, *Journal of Climate*, *24*(20), 5353–5364.

Held, I. M., R. S. Hemler, and V. Ramaswamy (1993), Radiative-convective equilibrium with explicit two-dimensional moist convection, *Journal of the Atmospheric Sciences*, *50*(23), 3909–3927.

Held, I. M., M. Winton, K. Takahashi, T. Delworth, F. Zeng, and G. K. Vallis (2010), Probing the fast and slow components of global warming by returning abruptly to preindustrial forcing, *Journal of Climate*, *23*(9), 2418–2427.

Hodzic, A., and J. P. Duvel (2018), Impact of biomass burning aerosols on the diurnal cycle of convective clouds and precipitation over a tropical island, *Journal of Geophysical Research: Atmospheres*, *123*(2), 1017–1036.

Hong, S.-Y., Y. Noh, and J. Dudhia (2006), A new vertical diffusion package with an explicit treatment of entrainment processes, *Monthly Weather Review*, *134*(9), 2318–2341.

Jeevanjee, N., and D. M. Romps (2013), Convective self-aggregation, cold pools, and domain size, *Geophysical Research Letters*, *40*(5), 994–998.

Kopparla, P., E. M. Fischer, C. Hannay, and R. Knutti (2013), Improved simulation of extreme precipitation in a high-resolution atmosphere model, *Geophysical Research Letters*, *40*(21), 5803–5808.

Lee, S. S., J. Guo, and Z. Li (2016), Delaying precipitation by air pollution over the Pearl River Delta: 2. Model simulations, *Journal of Geophysical Research: Atmospheres*, *121*(19).

Lilly, D. K. (1968), Models of cloud-topped mixed layers under a strong inversion, *Quarterly Journal of the Royal Meteorological Society*, *94*(401), 292–309.

Lin, Y.-L., R. D. Farley, and H. D. Orville (1983), Bulk parameterization of the snow field in a cloud model, *Journal of Climate and Applied Meteorology*, *22*(6), 1065–1092.

Lutsko, N. J., and T. W. Cronin (2018), Increase in precipitation efficiency with surface warming in radiative-convective equilibrium, *Journal of Advances in Modeling Earth Systems*.

Ming, Y., V. Ramaswamy, and G. Persad (2010), Two opposing effects of absorbing aerosols on global-mean precipitation, *Geophysical Research Letters*, *37*, L13701.

Muller, C., and S. Bony (2015), What favors convective aggregation and why?, *Geophysical Research Letters*, *42*(13), 5626–5634.

Muller, C. J., and I. M. Held (2012), Detailed investigation of the self-aggregation of convection in cloud-resolving simulations, *Journal of the Atmospheric Sciences*, *69*(8), 2551–2565.

Myhre, G., D. Shindell, F.-M. Bréon, W. Collins, J. Fuglestvedt, J. Huang, D. Koch, J.-F. Lamarque, D. Lee, B. Mendoza, T. Nakajima, A. Robock, G. Stephens, T. Takemura, and H. Zhang (2013), *Anthropogenic and Natural Radiative Forcing*, chap. 8, pp. 659–740, Cambridge University Press, Cambridge, United Kingdom and New York, NY, USA, doi:10.1017/CBO9781107415324.018.

O'Brien, T. A., W. D. Collins, K. Kashinath, O. Rübel, S. Byna, J. Gu, H. Krishnan, and P. A. Ullrich (2016), Resolution dependence of precipitation statistical fidelity in hindcast simulations, *Journal of Advances in Modeling Earth Systems*, *8*(2), 976–990.

O'Gorman, P. A. (2015), Precipitation extremes under climate change, *Current Climate Change Reports*, *1*(2), 49–59.

Pauluis, O., and S. Garner (2006), Sensitivity of radiative–convective equilibrium simulations to horizontal resolution, *Journal of the Atmospheric Sciences*, *63*(7), 1910–1923.

Richardson, T. B., P. M. Forster, T. Andrews, and D. J. Parker (2015), Understanding the rapid precipitation response to CO_2 and aerosol forcing on a regional scale, *J. Climate*, (2015).

Romps, D. M. (2017), Exact expression for the lifting condensation level, *Journal of the Atmospheric Sciences*, *74*(12), 3891–3900.

Rutledge, S. A., and P. V. Hobbs (1984), The mesoscale and microscale structure and organization of clouds and precipitation in midlatitude cyclones. XII: A diagnostic modeling study of precipitation development in narrow cold-frontal rainbands, *Journal of the Atmospheric Sciences*, *41*(20), 2949–2972.

Sillmann, J., V. Kharin, X. Zhang, F. Zwiers, and D. Bronaugh (2013), Climate extremes indices in the CMIP5 multimodel ensemble: Part 1. model evaluation in the present climate, *Journal of Geophysical Research: Atmospheres*, *118*(4), 1716–1733.

Sillmann, J., C. W. Stjern, G. Myhre, and P. M. Forster (2017), Slow and fast responses of mean and extreme precipitation to different forcing in CMIP5 simulations, *Geophysical Research Letters*, *44*(12), 6383–6390.

Stephens, G. L., T. L'Ecuyer, R. Forbes, A. Gettelmen, J.-C. Golaz, A. Bodas-Salcedo, K. Suzuki, P. Gabriel, and J. Haynes (2010), Dreary state of precipitation in global models, *Journal of Geophysical Research: Atmospheres*, *115*(D24).

Strong, J. D., G. A. Vecchi, and P. Ginoux (2015), The response of the tropical Atlantic and West African climate to Saharan dust in a fully coupled GCM, *Journal of Climate*, *28*(18), 7071–7092.

Takahashi, K. (2009), Radiative constraints on the hydrological cycle in an idealized radiative–convective equilibrium model, *Journal of the Atmospheric Sciences*, *66*(1), 77–91.

Tennekes, H. (1973), A model for the dynamics of the inversion above a convective boundary layer, *Journal of the Atmospheric Sciences*, *30*(4), 558–567.

Tompkins, A. M., and A. G. Semie (2017), Organization of tropical convection in low vertical wind shears: role of updraft entrainment, *Journal of Advances in Modeling Earth Systems*, *9*(2), 1046–1068.

Wang, S., and A. H. Sobel (2011), Response of convection to relative sea surface temperature: Cloud-resolving simulations in two and three dimensions, *Journal of Geophysical Research: Atmospheres*, *116*(D11).

Wilcox, E. M., and L. J. Donner (2007), The frequency of extreme rain events in satellite rain-rate estimates and an atmospheric general circulation model, *Journal of Climate*, *20*(1), 53–69.

Wing, A. A., K. Emanuel, C. E. Holloway, and C. Muller (2017), Convective self-aggregation in numerical simulations: a review, *Surveys in Geophysics*, pp. 1–25.

Zhao, M. (2014), An investigation of the connections among convection, clouds, and climate sensitivity in a global climate model, *Journal of Climate*, *27*(5), 1845–1862.